# On The Performance of The Effects of Temperature Variation in Ultrafast Incoherent Fiber-Optic CDMA Systems with SOA-Based Tunable Dispersion Compensator

**Che-Wei Chang**[1], **Guu-Chang Yang**[1], ***Fellow, IEEE***, **Ivan Glesk**[2], ***Senior Member, IEEE***, **Wing C. Kwong**[3], ***Senior Member, IEEE***

[1] *Department of Electrical Engineering and Graduate Institute of Communication Engineering, National Chung Hsing University, Taichung 402, Taiwan.*
[2] *Center for Intelligent and Dynamic Communications, Electronic and Electrical Engineering Department, University of Strathclyde, Glasgow, G1 1XW, United Kingdom.*
[3] *Department of Engineering, Hofstra University, Hempstead, NY 11549, USA.*

*DOI: 10.1109/JPHOT.2019.XXXXXXX*


Manuscript received January 10, 2019; revised April 13, 2019. First published May ??, 2019. Current version published ???? ??, 2019. Part of this paper was presented in ICTON 2019, Angers, France, July 9-13, 2019. This research was supported in part by the Ministry of Science and Technology of Republic of China under Grants MOST 105-2221-E-005-007-MY3, in part by the European Union's Horizon 2020 research and innovation program under the Marie Sklodowska-Curie grant agreement No 734331, and in part by the Faulty Development and Research Grants of Hofstra University.

**Abstract:** Recent studies show that temperature variation in ultrafast incoherent fiber-optic code-division multiple-access (FO-CDMA) systems using picosecond multiwavelength codes is a realistic problem even though dispersion-compensating fiber is utilized. The phenomenon creates distortions in auto- and cross-correlation functions and then worsens system performance. A physical-layer mitigation approach has been reported by using a recent demonstrated semiconductor-optical-amplifier-based tunable dispersion compensator to fully recover the auto-correlation peaks. Applying the concept of "chip granularity" to account for the effects of temperature variation to the cross-correlation functions, this paper formulates a new performance-analytical model for such FO-CDMA systems. The model also supports adjustable quality-of-services through code weight control.

**Index Terms:** code division multiple access, dispersion compensation, optical fiber communications, temperature variation

## 1. Introduction

In addition to wavelength-division and orthogonal frequency-division multiplexing, incoherent code-division multiple-access (CDMA) has been receiving attention in fiber-optic communication systems because the latter does not rely on complex electronic processing and can support asynchronous and uncoordinated multi-user access, bursty-type traffic, soft limit in the number of subscribers, and gradual performance deterioration under heavy load [1]–[3]. Multiuser fiber-optic code-division multiple-access (FO-CDMA) experimental testbeds operating at 10+ Gbit/s with bit-error-rate of less than $10^{-9}$ have been demonstrated [3]–[5]. Moreover, 2-D wavelength-time codes with good auto- and cross-correlation properties can provide scalability by coding in wavelength

and time and also support adjustable quality-of-services (QoS) by controlling code length and weight [1]–[7]. Recently, the effects of fiber temperature variation in ultrafast incoherent FO-CDMA systems using picosecond multiwavelength codes have been investigated [8]–[11]. They create time skew and dispersion in multiwavelength pulses and, in turn, destroy the integrities of autocorrection and cross-correlation functions seen at FO-CDMA receivers. Software and hardware approaches have been proposed to mitigate this kind of physical (temperature-induced) impairments [10]–[14].

In the software approach, the mitigation is performed in the data-link layer with power allocation schemes based on computational optimization algorithms [13], [14]. The power-allocation protocols were shown to be efficient and provide good performance-complexity trade-offs. In some applications, if real-time power adjustment of laser sources is not possible, one will need to fall back on the hardware approach. (In fact, both software and hardware approaches should be applied in tandem in order to support a variety of system environments.) Using the hardware approach in the physical layer, Ahmed, *et al.* [10]–[12] demonstrated a novel semiconductor-optical-amplifier (SOA)-based tunable dispersion compensator (TDC) to fine-tune dispersion compensation after a long fiber link equipped with dispersion-compensating fiber (DCF). In addition to removing residual CD after the DCF, another benefit of the SOA-based TDC is that it can fully compensate for the distortion of the autocorrelation peaks caused by fiber temperature variation without introducing extra hardware cost. Nevertheless, the temperature-induced distortion to the cross-correlation functions was not considered in the studies [10], [11]. As FO-CDMA system performance is determined by the receiver's ability to discriminate the autocorrelation peaks from the cross-correlation functions, a complete performance-analytical model needs to account for the distorted cross-correlation functions seen at the TDC output [9].

In this paper, an ultrafast incoherent FO-CDMA system using picosecond multiwavelength codes with optical signal processing, optical power thresholding, and the SOA-based TDC is overviewed in Section 2. The effects of fiber temperature variation to the cross-correlation functions in such a FO-CDMA system are also studied and related to the concept of "chip granularity" [7]. In Section 3, a new performance-analytical model of this FO-CDMA system with adjustable QoS is formulated. In Section 4, numerical examples and computer simulation are studied to validate the new model. Finally, conclusion is given in Section 5.

## 2. FO-CDMA System Model and Fiber-Temperature-Variation Effects

Fig. 1 shows an ultrafast incoherent (asynchronous) FO-CDMA system model, which consists of multiple stations (or users) connecting to a long fiber link. In a transmitter, a supercontinuum mode-locked laser is used to generate a train of picosecond multiwavelength pulses with a repetition rate of one pulse per bit period [5], [3]. Using on-off-keying (OOK) modulation, every data bit of "1" will turn on an optical modulator to let pass one such multiwavelength pulse to an optical encoder. In the encoder, the pulse is first wavelength split and spectrally sliced into $w$ single-wavelength pulses. They are then time-delayed accordingly to generate the (address) codeword of the intended receiving station [3], [2]. As CD is accumulated during long-distance transmission of these picosecond multiwavelength codewords, a DCF module is utilized at the end of the fiber link. Each receiver decodes the arrival codewords, distinguishes the correct codeword from interfering ones, and finally recovers the transmitted data bits. If an arrival codeword matches with the address codeword of the optical decoder, the $w$ pulses of the correct codeword will be realigned on top of each other within one chip. An autocorrelation function with a high peak of power (or height) $w$ will be created if there is no distortion caused by CD or temperature variation. An optical power thresholder [15], [16] will be triggered to generate a data bit of "1" whenever its input power level is at least $w$.

After the DCF module, a residual amount of dispersion may still exist. In addition, temperature differences among the stations as well as temperature variation encountered in the fiber link introduce extra amounts of time skew and dispersion to the mutliwavelength pulses. Ahmed,

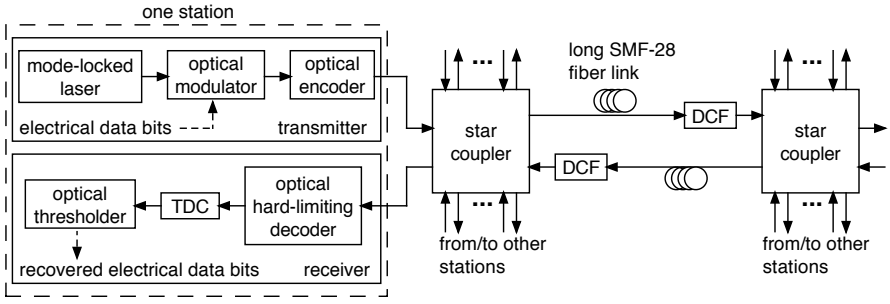


Fig. 1. An ultrafast incoherent (asynchronous) FO-CDMA system with the DCF and SOA-based TDC modules for tunable dispersion compensation.

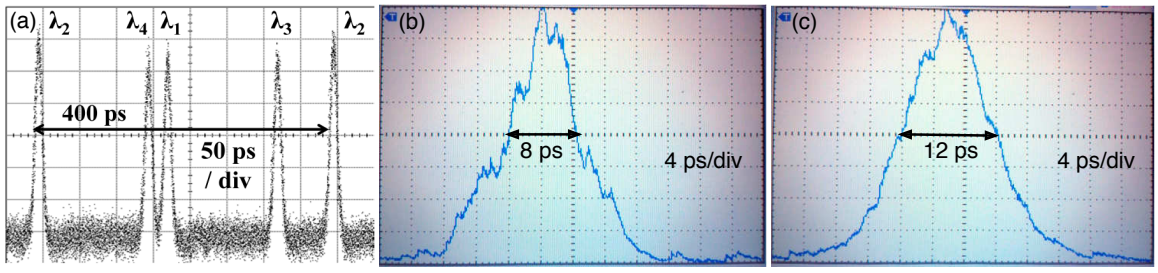


Fig. 2. Recovery of an autocorrelation peak of $12$ ps (FWHM) at the TDC output caused by $40°$C temperature variation in a $19.5$-km CD-compensated fiber link. (a) a multiwavelength codeword of $w = 4$ with 33 chips, chip-width of $12$ ps, and period of $400$ ps; (b) a distorted autocorrelation peak of $8$ ps (FWHM); (c) the recovered autocorrelation peak. (Note: The power levels of the two autocorrelation peaks are not the same; the vertical scale of the oscilloscope has been adjusted to maximize the waveform display after the measurement of a Femtochrome's optical autocorrelator.)

*et al.* [10]–[12] recently demonstrated the SOA-based TDC to achieve precise and dynamic dispersion compensation. The SOA's input-power sensitivity can be tuned to the power level of the autocorrelation peaks. This, in turn, triggers the gain-compression mechanism to compensate for the temperature-induced time skew and dispersion. For example, Fig. 2(a) shows an optical codeword generated by an optical encoder with fiber-Bragg-gratings (FBG) [2]. It consists of optical pulses of $12$ ps (FWHM) and four wavelengths $\lambda_1 = 1,550.12$, $\lambda_2 = 1,550.92$, $\lambda_3 = 1,551.72$, and $\lambda_4 = 1,552.52$ nm, spreading over a period of $400$ ps. These correspond to chip-width of $12$ ps, code length of $33$ chips, and $2.5$ Gbit/s data rate. Fig. 2(b) shows the distorted autocorrelation peak caused by $40°$C temperature variation in a $19.5$-km CD-compensated fiber link, which includes a portion of DCF to fully compensate for CD. Thus, Fig. 2(b) shows the net effect of fiber temperature variation, which distorts the autocorrelation peak to $8$ ps (FWHM). Fig. 2(c) shows the corrected autocorrelation peak, which is fully compensated back to $12$ ps at the SOA-based TDC output.

It is important to point out that fiber temperature variation also creates distortion to the cross-correlation function (from multiple interfering codewords) [9]. As the distorted cross-correlation function generally has much lower power than the autocorrelation peak, it cannot trigger the TDC to compensate for the distortion. Moreover, the effects of distorted cross-correlation function after the TDC were not studied [10]–[12]. Without such information, system performance cannot be studied accurately [9].

### *2.1. Effects of Fiber Temperature Variation*

Assume that the multiwavelength pulses from the mode-locked laser are modeled with a hyperbolic-secant-squared ($\text{sech}^2$) pulse envelope. With fiber temperature variation, the "energy-normalized"

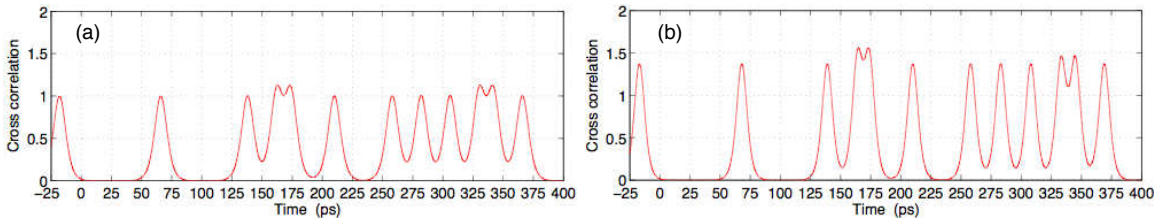


Fig. 3. Cross-correlation functions seen at the decoder of $X_1 = (0, 7, 14, 21)$ created by the interfering $(4 \times 31, 4, 1)$ CHPC codewords of $X_2 = (0, 5, 10, 15)$, $X_3 = (0, 13, 26, 8)$, and $X_4 = (0, 23, 15, 7)$ of chip-width $t_c = 12$ ps after the codewords have traveled in a CD-compensated fiber of $d = 19.5$ km experiencing (a) $\Delta T = 0°$C and (b) $\Delta T = 40°$C. The time origins of $X_3$ is right-shifted by 4 chips and $X_4$ is right-shifted by 7 chips to simulate the asynchronous nature of the CHPCs. (This example corresponds to chip granularity of $g = 12$ in the proposed time-skew analytical model.)

sech$^2$ pulse envelope of the $k$th wavelength can generally be written as [8], [9]

$$S_k(t) = \frac{\sigma}{\sigma - \Delta\sigma} \text{sech}^2 \left( \frac{t - k\Delta t}{\sigma - \Delta\sigma} \right) \tag{1}$$

with the temperature-induced time skew $\Delta t$ and dispersion $\Delta\sigma$ given by

$$\Delta t = D_{\text{temp}} \times \Delta T \times \Delta\Lambda \times d \quad \text{(ps)} \tag{2}$$

$$\Delta\sigma = D_{\text{temp}} \times \Delta T \times \Delta\lambda \times d \quad \text{(ps)} \tag{3}$$

respectively, where $k \in [0, w-1]$ and $w$ is the number of multiwavelength pulses (i.e., weight) in each codeword. $D_{\text{temp}}$ (ps/nm/km/°C) is the fiber thermal coefficient. $\Delta T$ (°C) is the temperature variation encountered in a fiber link of $d$ (km). The multiwavelength pulses have spectral linewidth $\Delta\lambda$ (nm) and full-width at half-maximum (FWHM) duration $t_c \approx 1.76\sigma$ (i.e., chip-width of codewords), and $\sigma$ is called the duration of the sech$^2$ pulse. The wavelengths are here assumed equally spacing by $\Delta\Lambda$ (nm) with $\lambda_0 < \lambda_1 < \cdots < \lambda_{w-1}$.

While there exist other wavelength-time codes, such as 2-D optical orthogonal codes [2] and modified double weight codes [17], the carrier-hopping prime codes (CHPCs) are used for illustration in this paper because they are created by a simple algebraic algorithm and designed for asynchronous multi-user operation with ideal zero autocorrelation sidelobe and (in-phase and out-of-phase) cross-correlation functions of at most one [1], [2]. Illustrating with the $(L \times N, w, \theta_c) = (4 \times 31, 4, 1)$ CHPCs, each codeword consists of $N = 31$ time slots (or chips), $L = 4$ wavelengths, weight $w = 4$ (i.e., pulses), and the (ideal) maximum cross-correlation function of $\theta_c = 1$. They are assumed to have chip-width $t_c = 12$ ps, pulse duration $\sigma = 6.82$ (i.e., FWHM width $= 1.76 \times 6.82 = 12$ ps), spectral linewidth $\Delta\lambda = 0.8$ nm, spectral spacing $\Delta\Lambda = 0.8$ nm, and fiber thermal coefficient $D_{\text{temp}} = 0.0016$ ps/nm/km/°C. Caused by fiber temperature variation of $\Delta T = 40°$C in a CD-compensated fiber link of $d = 19.5$ km, (2) and (3) give time skew of $\Delta t = 1.00$ ps and dispersion of $\Delta\sigma = 1.00$ ps. Thus, the pulses of each codeword are equally compressed from $12$ ps to $1.76(\sigma - \Delta\sigma) = 10.24$ ps (FWHM). The pulse of wavelength $\lambda_k$ is time-skewed by $k\Delta t = k$ ps for $k \in [0, 3]$.

Fig. 3 shows the (a) original and (b) distorted cross-correlation functions at the decoder output of $X_1 = (0, 7, 14, 21)$ caused by interfering $(4 \times 31, 4, 1)$ CHPC codewords of $X_2 = (0, 5, 10, 15)$, $X_3 = (0, 13, 26, 8)$, and $X_4 = (0, 23, 15, 7)$ without and with fiber temperature variation, respectively, based on the above parameters. (The 4-tuple of each codeword denotes the time-slot positions of $\lambda_0$, $\lambda_1$, $\lambda_2$, and $\lambda_3$, correspondingly.) As shown in Fig. 3(a), the original height of the cross-correlation function is equal to 1 unit of power because the CHPCs have ideal $\theta_c = 1$. With fiber temperature variation, the dispersion increases the height (i.e., power) of the compressed pulses to about $1.38$ units and the time skew causes adjacent pulses (around $170$ ps) to overlap and further worsens the distorted cross-correlation value to above 1.5 units. These equivalently give

$\theta_c \geq 1.38$, at least 38% increment in the cross-correlation value, and translate to poorer system performance (see Section 3) even with the TDC to perfectly recover the autocorrelation peak.

Because the pulses of each wavelength are regularly time-skewed by an integral multiple of $\Delta t$, the pattern can equivalently be modeled by subdividing each chip (of chip-width $t_c$) into sub-chip of width $\Delta t$. In generally, the temperature-induced time-skewed version of codeword $X$ can be denoted as $X' = (t_0, t_1 - \Delta t, t_2 - 2\Delta t, \ldots, t_{w-1} - (w-1)\Delta t)$. Borrowing the concept of *chip granularity* [7], this is equivalent of having the chip granularity $g = \lfloor t_c/\Delta t \rceil$, where $\lfloor \cdot \rceil$ is a function of rounding a real number to the nearest integer. Using chip granularity $g$ to denote the number of equal-width sub-chips in each chip, it is an important parameter in the new time-skew analytical model in Section 3. Using the above example, with $\Delta\lambda = \Delta t = 1.00$ ps and $t_c = 12$ ps, the problem can be treated by the proposed time-skew model with $g = 12$. Using the same parameters but $d = 30$ km, $\Delta\lambda = \Delta t = 1.536$ ps result in larger time skew and dispersion and thus more distortion in the cross-correlation function. These, in turn, give a smaller chip granularity $g \approx 8$ in the proposed time-skew model. As shown in Section 3, a larger $g$ gives a better system performance, and this is consistent with the observations in this section.

## 3. New Time-Skew Performance-Analytical Model

In general, the hard-limiting error probability of a family of $(L \times N, w, \theta_c)$ 2-D optical codes in incoherent (asynchronous) FO-CDMA systems with OOK modulation is given by [1], [2]

$$P_e = \frac{1}{2}\sum_{i=0}^{w}(-1)^{w-i}\binom{w}{i}\left[\sum_{j=0}^{\theta_c}\frac{\binom{i}{j}}{\binom{w}{j}}q_{\theta_c,j}\right]^{K-1} \tag{4}$$

where $K$ represents the number of simultaneous users and $q_{\theta_c,j}$ denotes the probability of getting $j \in [0, \theta_c]$ hits in the cross-correlation function at a decision time. These hit probabilities are generally related by $\sum_{j=0}^{\theta_c} q_{\theta_c,j} = 1$ and $\sum_{j=0}^{\theta_c} j q_{\theta_c,j} = w^2/(2LN)$ [1], [2].

According to Section 2.1, the time skews of multiwavelength pulses in codewords can equivalently be modeled as dividing every chip (of width $t_c$) into $g = \lfloor t_c/\Delta t \rceil$ equal-width sub-chips. In the new time-skew model, whenever at least one sub-chip in a mark chip of the distorted cross-correlation function is hit by an interfering pulse, this partial hit will be considered as one "valid" hit. New valid-hit probabilities, $q'_{\theta_c,j,g}$, for the $(L \times N, w, 1)$ CHPCs are formulated, where $q'_{\theta_c,j,g}$ represents the probability of getting $j \in [0, \theta_c]$ valid hits in the distorted cross-correlation function. Afterward, the actual hit probabilities, $q_{\theta_c,j,g}$, are calculated by multiplying $q'_{\theta_c,j,g}$ with scaling factors in order to reflect the actual (power) contribution of these partial hits. Besides better quantifying the actual effects of the distorted cross-correlation function (in terms of $w$ and $g$) in ultrafast incoherent FO-CDMA systems with the SOA-based TDC than the old fixed-QoS pulse-random-shift model [9], the new analytical model in the following theorem (with proofs in the Appendix) also applies, for the first time, to variable code weight for adjustable QoS.

**Theorem 1:**

To account for the actual effect of fiber temperature variation under the SOA-based TDC, the hit probabilities of the $(w \times p, w, 1)$ CHPCs in the new time-skew model with $w < p$ and $g \geq w$ can be formulated as

$$q_{2,0,g} = 1 - q_{2,1,g} - q_{2,2,g} \tag{5}$$

$$q_{2,1,g} = \frac{2w(p-w+1) - p - 1}{2p(p-1)} \times \frac{g}{2g-1} \tag{6}$$

$$q_{2,2,g} = \frac{(w-1)^2}{2p(p-1)} \times \frac{2g-1}{4(g-1)} \tag{7}$$

The hit probabilities of the $(p \times p, p, 1)$ CHPCs with $g \geq p$ can be formulated as

$$q_{2,0,g} = 1 - q_{2,1,g} - q_{2,2,g} = \frac{6g-1}{8g} \quad (8)$$

$$q_{2,1,g} = \frac{1}{2p} \times \frac{1}{2} \quad (9)$$

$$q_{2,2,g} = \frac{p-1}{2p} \times \frac{2g-1}{4(g-1)} \quad (10)$$

The hit probabilities the $(w \times p^2, w, 1)$ CHPCs with $w < p$ and $g \geq w$ can be formulated as

$$q_{2,0,g} = 1 - q_{2,1,g} - q_{2,2,g} \quad (11)$$

$$q_{2,1,g} = \frac{2w(p^2-w+1)-p^2-1}{2p^2(p^2-1)} \times \frac{g}{2g-1} \quad (12)$$

$$q_{2,2,g} = \frac{(w-1)^2}{2p^2(p^2-1)} \times \frac{2g+1}{4g} \quad (13)$$

The hit probabilities of the $(p \times p^2, p, 1)$ CHPCs with $g \geq p$ can be formulated as

$$q_{2,0,g} = 1 - q_{2,1,g} - q_{2,2,g} \quad (14)$$

$$q_{2,1,g} = \frac{2p^3-3p^2+2p-1}{2p^2(p^2-1)} \times \frac{g}{2g-1} \quad (15)$$

$$q_{2,2,g} = \frac{p-1}{2p^2(p+1)} \times \frac{2g-1}{4(g-1)} \quad (16)$$

Note that the first part in each of the above hit probabilities does not contain $g$ because there are always 2-valid-hits within the original mark chips of the distorted cross-correlation function due to the temperature-induced fixed-time-skew patterns. Rather, the scaling factors (in the second parts of the formulas) depend on $g$, as explained in the Appendix. These factors gradually decrease as $g$ increases because more portions of the hits will stay within the original mark chips. When $g$ approaches infinity (with infinitesimal temperature variation), the scaling factors become 1/2 and give the lowest (i.e., best) hit probabilities, in turn, resulting in the lower bound of error probability for the new time-skew model.

## 4. Numerical Results and Simulation

Fig. 4 compares the hard-limiting error probabilities, $P_e$ of (4), of the $(w \times p^2, w, 1)$ CHPCs in the new time-skew model, from (11)–(13), with various combinations of $w = \{5, 6, 7\}$, $p = \{7, 11, 13\}$, and $g = \{2, 3, 4, 8, 12, 30\}$. For baseline comparison, the dashed curves show the error probabilities of the $g = \infty$ case when there is no temperature variation. In general, the error probability (i.e., performance) gets worse as $K$ increases because of stronger interference. The performance improves as $w$ (or $N$) increases because heavier code weight (or longer code length) reduces the hit probabilities and also the former increases the power of the autocorrelation peak. The performance improves with $g$ and gradually approaches to the $P_e$ lower bound of $g = \infty$. As the temperature-induced time-skew patterns are regular and the sub-chip-width is proportional to $1/g$, more portions of the hits (created by interfering codewords) will occur within the original mark chips of the cross-correlation function when $g$ increases and $g \geq w$. In other words, the amount of partial hits falling into the adjacent chip decreases, resulting in less interference and, in turn, approaching the performance lower bound (i.e., dashed curves). Computer simulation is performed to validate the new time-skew analytical model. The simulation results (i.e., "$\times$" symbols) match closely with the analytical (solid) curves.

The computer simulation is based on the so-called Monte-Carlo simulation method. It begins with randomly assigning a distinct codeword to each user's receiver as its address signature. The

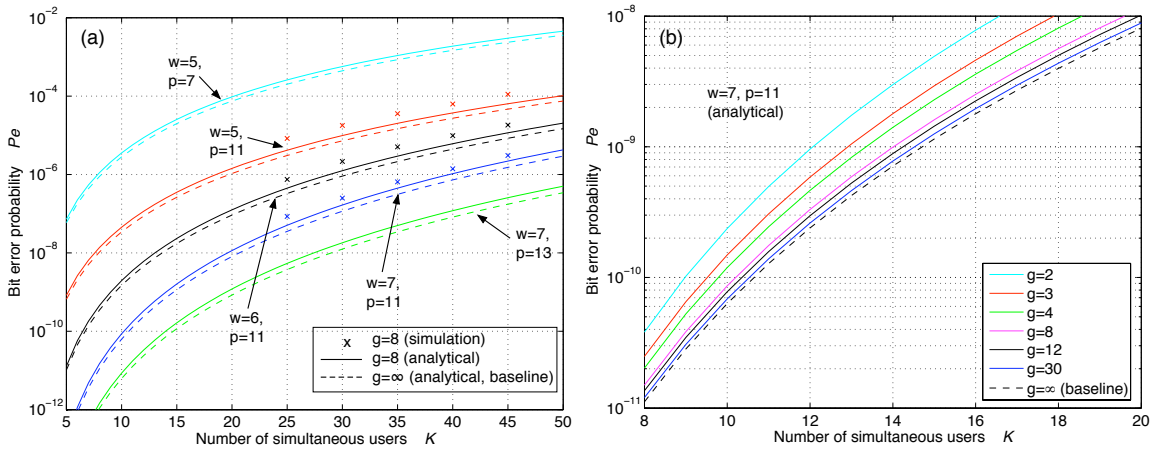


Fig. 4. Bit error probability $P_e$ in the new time-skew model versus the number of simultaneous users $K$ for the $(w \times p^2, w, 1)$ CHPCs with various combinations of $w = \{5, 6, 7\}$, $p = \{7, 11, 13\}$, and $g = \{2, 3, 4, 8, 12, 30\}$.

$K$ simultaneous users transmit the address codewords of their intended receivers when a data bit of 1 is conveyed. The time frame of the fiber link is divided into $N$ chips per bit period, and any simultaneous user can start to transmit its codeword at any chip to simulate bit-asynchronism in incoherent (asynchronous) FO-CDMA. According to the severity of fiber temperature variation, every chip is divided into $g$ sub-chips; the multiwavelength pulses in every codeword are time-delayed to these $g$ sub-chips, according to (2). In a receiver, if there are multiple pulses of the same wavelength (coming from multiple interfering codewords) arriving at the same chip, these pulses are hard-limited and only counted as one pulse (of that wavelength) at that chip. Afterward, correlation is performed by comparing the wavelengths in all $w$ mark chips of the address codeword of the receiver with the wavelengths and chip locations of the pulses of the hard-limited signal. If there exists a pulse with the wavelength and chip location matching one of the mark chips of the address codeword, "one hit" is added to the count. The total height (i.e., power) of the hits (sub-chip by sub-chip) at the $w$ mark chips of the address codeword is summed up. If the total power in one sub-chip within the expected chip-location of the autocorrelation peak is as high as $w$, a data bit of 1 will be recovered wrongly. Finally, the error probability is calculated as the ratio of the number of decision errors to the total number of transmitted data bits. For a given $K$, the number of data bits used is 100 times of the reciprocal of the targeting error probability in order to provide sufficient simulation iterations and randomness.

## 5. Conclusion

In this paper, the performance of an ultrafast incoherent FO-CDMA system, which used picosecond multiwavelength codes and was equipped with the SOA-based TDC, under the influence of fiber temperature variation was investigated and formulated by the new analytical model. The benefits of the model were two-folded: (1) it systematically quantified the deleterious influence of fiber temperature variation to the cross-correlation function and the beneficial effect of the TDC in terms of chip granularity; and (2) for the first time, it was applicable to arbitrary code weight for adjustable system QoS. Validated with computer simulation, the studies showed that the TDC's compensation capability for the distorted cross-correlation functions could be reflected by keeping chip granularity large, which, in turn, resulted in better system performance.

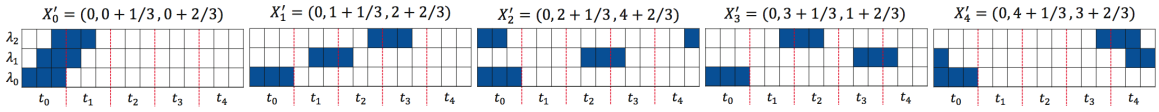


Fig. 5. $(3 \times 5, 3, 1)$ CHPCs with the regular time-skew patterns created by fiber temperature variation with $g = 3$.

# Appendix

## *A.1. Proof of (5)–(7) in the new time-skew model for the $(w \times p, w, 1)$ CHPCs*

When a pulse of an interfering codeword hits a mark chip of the address codeword with a correct wavelength, it is here treated as a "valid" hit, no matter the hit takes up a partial or whole chip. In the new time-skew model, every pulse of an interfering codeword is regularly time-skewed to start at one of the $g$ sub-chips in the pulse's original chip position, governed by $k\Delta t$ in (2). Because every codeword of length $N$ can have up to $N$ cyclic-shifts, the total number of all "valid" hits is found to be $g^w\phi(\phi-1)N/g^w = p(p-1)p$ in the time-skew model if $\phi = N = p$, where $\phi$ is the cardinality of the $(w \times N, w, 1)$ CHPCs.

In the correlation process, every arrival codeword correlates with the address codeword chip-by-chip sequentially [1], [2]. Without loss of generality, it is assumed that the pulse of wavelength $\lambda_0$ of every interfering codeword creates one full hit (i.e., taking up the whole chip) in the cross-correlation function with the address codeword at the mark chip of $\lambda_0$. Due to the regular sub-chip skews, the pulses of other (non-$\lambda_0$) wavelengths of every interfering codeword will partially hit other mark chips (of correct wavelengths) of the address codeword. In the model, this kind of partial hits is also treated as "valid" hits, in addition to the full hits from the $\lambda_0$-pulses.

Due to the CHPC structure and regular sub-chip skews, when an interfering codeword generates a valid hit at one wavelength in one chip location of the cross-correlation function, another (different-wavelength) pulse may also create a second valid hit in the same chip location. This scenario then creates a 2-valid-hit. To prevent 2-valid-hits from occurring, the $g^w$ possible starting locations for the $w$ pulses in each codeword need to be reduced to $g^{w-1}$. For example, Fig. 5 shows the time-skew patterns of the $(3 \times 5, 3, 1)$ CHPCs created by fiber temperature variation with $g = 3$. Assuming that original codeword $X_0 = (0, 0, 0)$ is used as the address codeword of the decoder. Because $X_0$ has pulses of wavelengths $\lambda_0$, $\lambda_1$, and $\lambda_2$ on top of each other (at chip $t_0$) by design, the cross-correlation process at this decoder simply looks at every arriving codeword to see if there are any (full and partial) pulse overlaps at the same chip location. For illustration, when the time-skewed codeword $X_1' = (0, 1+1/3, 2+2/3)$ arrives at this decoder, the $\lambda_0$-pulse at chip $t_0$ will generate the pattern "111" (i.e., full hit) and be counted as a 1-valid-hit in this chip location of the cross-correlation function. Similarly, the "011" pattern due to $\lambda_1$ at chip $t_1$ generates a 1-valid-hit in the next chip location. However, at chip $t_2$, the cross-correlation function sees two valid hits: one from the "100" pattern due to $\lambda_1$ and another from the "001" pattern due to $\lambda_2$. This scenario contributes a 2-valid-hit, giving a cross-correlation function of 2 in height (i.e., power). At chip $t_3$, the "110" pattern due to $\lambda_2$ contributes a 1-valid-hit. Finally, the empty chip at $t_4$ contributes a 0-valid-hit.

Applying the above counting method to all $(w \times p, w, 1)$ CHPC codewords, the number of 1-valid-hits is found to be $(2w + 2\phi w - 2w^2 - \phi - 1)N = (2w + 2pw - 2w^2 - p - 1)p$, and the number of 2-valid-hits is found to be $(w-1)^2N = (w-1)^2p$. Hence, for the $(w \times p, w, 1)$ CHPCs with temperature-induced time-skews, the 1-valid-hit and 2-valid-hit probabilities can be derived as

$$q'_{2,1,g} = \frac{1}{2} \times \frac{\text{number of 1-valid-hits}}{\text{total number of all valid hits}} = \frac{2w(p-w+1)-p-1}{2p(p-1)} \quad \text{(A.1)}$$

$$q'_{2,2,g} = \frac{1}{2} \times \frac{\text{number of 2-valid-hits}}{\text{total number of all valid hits}} = \frac{(w-1)^2}{2p(p-1)} \quad \text{(A.2)}$$

respectively, for $w < p$ and $g \geq w$.

Due to the regular sub-chip skews, the partial hits within one chip location in the cross-correlation function may not be able to stack up atop each other but side-by-side instead. This scenario only contributes one unit of pulse power rather than two. Two scaling factors, $g/(2g-1)$ and $(2g-1)/[4(g-1)]$, are multiplied to $q_{2,1,g}$ in (A.1) and $q_{2,2,g}$ in (A.2), respectively, in order to reflect the actual (power) contribution of these partial hits of the $(w \times p, w, 1)$ CHPCs. After some manipulations, (6) and (7) are formulated.

These two scaling factors are derived by counting all possible time-skew patterns of the partial hits in the cross-correlation functions of the $(w \times p, w, 1)$ CHPCs. Using the same example in Fig. 5, the (partial and full) hits contributed by the hit patterns "111," "110," "011," "001," and "100," with equal occurrence probability of $1/5$, are counted as 1-valid-hits. So, the expected value becomes $(3/3) \times (1/5) + (2/3) \times (1/5) + (2/3) \times (1/5) + (1/3) \times (1/5) + (1/3) \times (1/5) = 3/5$, which can equivalently be written as $g/(2g-1)$ for $g = 3$. The (partial and full) hits contributed by "101" (from "100 + 001"), "221" (from "111 + 110"), "211" (from "111 + 100"), and "121" (from "111 + 010"), with equal occurrence probability of $1/4$, are counted as 2-valid-hits. So, the expected value becomes $(2/6) \times (1/4) + (4/6) \times (1/4) + (4/6) \times (1/4) + (5/6) \times (1/4) = 5/8$, which can equivalently be written as $(2g-1)/[4(g-1)]$ for $g = 3$.

### A.2. Proof of (8)–(10) in the new time-skew model for the $(p \times p, p, 1)$ CHPCs

The derivations of the hit probabilities of the $(p \times p, p, 1)$ CHPCs in the new time-skew model are identical to those of the $(w \times p, w, 1)$ CHPCs by applying $w = p$ into (A.1) and (A.2). The two scaling factors for 1- and 2-valid-hits now become $1/2$ and $(2g-1)/[4(g-1)]$, respectively. They are derived by counting all possible time-skew patterns of the partial hits in the cross-correlation functions of the $(p \times p, p, 1)$ CHPCs. For example, considering all cases of $g = 3$, the (partial and full) hits contributed by the hit-patterns "011" and "001," with equal occurrence probability of $1/2$, are counted as 1-valid-hits. So, the expected value becomes $(2/3) \times (1/2) + (1/3) \times (1/2) = 1/2$, which can be equivalently be written as $1/2$ for $g = 3$. The (partial and full) hits contributed by the patterns "221" (from "110 + 111"), "101" (from "100 + 001"), "211" (from "100 + 111"), and "121" (from "110 + 011"), with equal occurrence probability of $1/4$, are counted as 2-valid-hits. So, the expected value become $(5/6) \times (1/4) + (4/6) \times (1/4) + (4/6) \times (1/4) + (2/6) \times (1/4) = 15/24$, which can be equivalently be written as $(2g-1)/[4(g-1)]$ for $g = 3$.

### A.3. Proof of (11)–(13) in the new time-skew model for the $(w \times p^2, w, 1)$ CHPCs

The derivations of the hit probabilities of the $(w \times p^2, w, 1)$ CHPCs in the new time-skew model are similar to those of the above derivations. The total number of all "valid" hits now becomes $g^w \phi(\phi-1)N/g^w = p^2(p^2-1)p^2$ as $\phi = N = p^2$.

By inspection, the $(w \times p^2, w, 1)$ CHPCs have three scenarios of creating 1- and 2-valid hits, where $w \leq p$. Scenario 1 consists of the codewords that are the same as the $p$ codewords of the $(w \times p, w, 1)$ CHPCs. Scenario 2 consists of codewords that contain the element of $p^2 - 1$ (i.e., having a pulse at the last chip $t_{p^2-1}$). Scenario 3 contains the remaining codewords in the set of $(w \times p^2, w, 0, 1)$ CHPCs. For example, the $(w \times 3^2, w, 1)$ CHPCs have $3^2$ codewords, in which codewords $(0,0,0)$, $(0,1,2)$, and $(0,2,1)$ belong to scenario 1, codewords $(0,4,8)$ and $(0,8,4)$ are in scenario 2, and codewords $(0,3,6)$, $(0,6,3)$, $(0,7,5)$, and $(0,5,7)$ go to scenario 3. The reasons of dividing the codewords into three scenarios are that (i) scenario 1 contains 2-valid-hits from those resemble to the $(w \times p, w, 1)$ CHPCs, (ii) scenario 2 consists of 2-valid-hits caused by one pulse at the first chip $t_0$ and another pulse at last chip $t_{p^2-1}$, and (iii) scenario 3 does not carry any 2-valid-hits.

Combining the three scenarios, the numbers of 1- and 2-valid-hits are found to be $[2w(p^2-w+1)-p^2-1]p^2$ and $(w-1)^2p^2$, respectively. Hence, for the $(w \times p^2, w, 1)$ CHPCs with temperature-induced time-skews, 1-valid-hit and 2-valid-hit probabilities can be derived as

$$q'_{2,1,g} = \frac{1}{2} \times \frac{\text{total number of 1-valid-hits in 3 scenarios}}{\text{total number of all valid-hits}} = \frac{[2w(p^2-w+1)-p^2-1]p^2}{2p^2(p^2-1)p^2} \quad \text{(A.3)}$$

$$q'_{2,2,g} = \frac{1}{2} \times \frac{\text{total number of 2-valid-hits in 3 scenarios}}{\text{total number of all valid-hits}} = \frac{(w-1)^2}{2p^2(p^2-1)} \quad \text{(A.4)}$$

Afterward, two scaling factors, $g/(2g-1)$ and $(2g+1)/(4g)$, are multiplied to $q'_{2,1,g}$ in (A.3) and $q'_{2,2,g}$ in (A.4), respectively, in order to reflect the actual (power) contribution of these partial hits. After some manipulations, (12) and (13) are formulated.

The two scaling factors are derived by counting all possible time-skew patterns of the partial hits in the cross-correlation functions of the $(w \times p^2, w, 1)$ CHPCs. Using the same example of the $(w \times 3^2, w, 1)$ CHPCs with $g = 3$ and $w \leq 3$, the (partial and full) hits contributed by the hit-patterns "111," "011," "001," "100," and "110," with equal occurrence probability of $1/5$, are counted as 1-valid-hits. So, the expected value becomes $(3/3) \times (1/5) + (2/3) \times (1/5) + (2/3) \times (1/5) + (1/3) \times (1/5) + (1/3) \times (1/5) = 3/5$, which can equivalently be written as $g/(2g-1)$ for $g = 3$. The (partial and full) hits contributed by "211" (from "111 + 100"), "221" (from "111 + 110"), "121" (from "110 + 011"), "101" (from "100 + 001"), and "111" (from "100 + 011" and "110 + 001"), with equal occurrence probability of $1/6$, are counted as 2-valid-hits. So, the expected value becomes $(5/6) \times (1/6) + (4/6) \times (1/6) + (4/6) \times (1/6) + (2/6) \times (1/6) + (3/6) \times (2/6) = 7/12$, which can equivalently be written as $(2g+1)/(4g)$ for $g = 3$.

### *A.4. Proof of (14)–(16) in the new time-skew model for the $(p \times p^2, p, 1)$ CHPCs*

The derivations of the hit probabilities of the $(p \times p^2, p, 1)$ CHPCs in the new time-skew model are identical to those of the $(w \times p^2, w, 1)$ CHPCs by applying $w = p$ into (A.3) and (A.4). The two scaling factors for 1- and 2-valid-hits now become $g/(2g-1)$ and $(2g-1)/[4(g-1)]$, respectively. They are derived by counting all possible time-skew patterns of the partial hits in the cross-correlation functions of the $(p \times p^2, p, 1)$ CHPCs. For example, using the $(3 \times 3^2, 3, 1)$ CHPCs with $g = 3$, the (partial and full) hits contributed by the hit-patterns "111," "011," "001," "100," and "110," with equal occurrence probability of $1/5$, are counted as 1-valid-hits. So, the expected value becomes $(3/3) \times (1/5) + (2/3) \times (1/5) + (2/3) \times (1/5) + (1/3) \times (1/5) + (1/3) \times (1/5) = 3/5$, which can equivalently be written as $g/(2g-1)$ for $g = 3$. The (partial and full) hits contributed by "211" (from "111 + 100"), "221" (from "111 + 110"), "121" (from "110 + 011"), and "101" (from "100 + 001"), with equal occurrence probability of $1/4$, are counted as 2-valid-hits. So, the expected value becomes $(5/6) \times (1/4) + (4/6) \times (1/4) + (4/6) \times (1/4) + (2/6) \times (1/4) = 5/8$, which can equivalently be written as $(2g-1)/[4(g-1)]$ for $g = 3$.

## References


[1] G.-C. Yang and W.C. Kwong, *Prime Codes with Applications to CDMA Optical and Wireless Networks*, Norwood, MA: Artech House, 2002.

[2] W.C. Kwong and G.-C. Yang, *Optical Coding Theory with Prime*, New York: CRC Press, 2013.

[3] *Optical Code Division Multiple Access: Fundamentals and Applications*, ed. P.R. Prucnal, Boca Raton, FL: Taylor & Francis, 2006.

[4] V.J. Hernandez *et al.*, "A 320-Gb/s capacity (32-user × 10 Gb/s) SPECTS O-CDMA network testbed with enhanced spectral efficiency through forward error correction," *J. Lightw. Technol.*, vol. 25, no. 1, pp. 79–86, Jan. 2007.

[5] C.-S. Brès, I. Glesk, and P.R. Prucnal, "Demonstration of an eight-user 115-Gchip/s incoherent OCDMA system using supercontinuum generation and optical time gating," *IEEE Photon. Technol. Lett.*, vol. 18, no. 7, pp. 889–891, Apr. 2006.

[6] W.C. Kwong, P.A. Perrier, and P.R. Prucnal, "Performance comparison of asynchronous and synchronous code-division multiple-access techniques for fiber-optic local area networks," *IEEE Trans. Commun.*, vol. 39, no. 11, pp. 1625–1634, Nov. 1991.

[7] Y.-T. Lin, G.-C. Yang, C.-Y Chang, and W.C. Kwong, "Design and analysis of asynchronous incoherent optical-CDMA systems using a new code-shifting technique," *IEEE Trans. Commun.*, vol. 63, no. 7, pp. 2619–2631, Jul. 2015.

[8] T.B. Osadola, S.K. Idris, I. Glesk, and W.C Kwong, "Effect of variations in environmental temperature on 2D-WH/TS OCDMA code performance," *J. Opt. Commun. Netw.*, vol. 5, no. 1, pp. 68–73, Jan. 2013.

[9] C.-Y. Tsai, G.-C. Yang, J.-S. Lin, C.-Y. Chang, I. Glesk, and W.C. Kwong, "Pulse-power-detection analysis of incoherent O-CDMA systems under the influence of fiber temperature fluctuations," *J. Lightw. Technol.*, vol. 35, no. 12, pp. 2366–2379, Jun. 2017.

[10] M.S. Ahmed, M.S.K. Abuhelala, and I. Glesk, "Managing dispersion-affected OCDMA auto-correlation based on PS multiwavelength code carriers using SOA," *J. Opt. Commun. Netw.*, vol. 9, no. 8, pp. 693–698, Aug. 2017.

[11] M.S. Ahmed and I. Glesk, "Mitigation of temperature-induced dispersion in optical fiber on OCDMA auto-correlation," *IEEE Photon. Technol. Lett.*, vol. 29, no. 22, pp. 1979–1982, Nov. 15, 2017.
[12] M.S. Ahmed and I. Glesk, "Management of OCDMA auto-correlation width by chirp manipulation using SOA," *IEEE Photon. Technol. Lett.*, vol. 30, no. 9, pp. 785–789, May 2018.
[13] A.J. dos Santos, F.R. Durand, and T. Abrão, "Mitigation of environmental temperature variation effects in OCDMA networks using PSO power control," *IEEE/OSA J. Opt. Commun. Netw.*, vol. 7, no. 8, pp. 707–717, Aug. 2015.
[14] T.D.S. Cavalia, F.R. Durand, P. Scalassaraa, and T. Abrão, "Power allocation scheme for mitigation of fiber temperature fluctuations in OCDMA networks based on firefly algorithm," *Opt. Switch. Network.*, vol. 30, pp. 1–9, Nov. 2018.
[15] K. Kravtsov, P.R. Prucnal, and M.M. Bubnov, "Simple nonlinear interferometer-based all-optical thresholder and its applications for optical CDMA," *Optics Express*, vol. 15, no. 20, pp. 13114–13122, 26 Sep. 2007.
[16] I. Glesk, P.R. Prucnal, and I. Andonovic, "Incoherent ultrafast OCDMA receiver design with 2 ps all-optical time gate to suppress multiple-access interference," *IEEE J. Select. Top. Quant. Electron.*, vol. 14, no. 3, pp. 861–867, May/Jun. 2008.
[17] I.S. Ahmed, S.A. Aljunid, C.B.M. Rashidi, and L.A.Khalil, "Performance evaluation analysis of wavelength/time 2-D modified double weight code In OCDMA," in *proc. Inter. Conf. Electron, Computer Info. Technol.*, Jan. 5-6, 2016, Kuala Lumpur, Malaysia.